




Molecular determinants for the chemical activation of the warmth-sensitive TRPV3 channel by the natural monoterpene carvacrol

Received for publication, October 5, 2021, and in revised form, January 31, 2022. Published, Papers in Press, February 9, 2022.

<https://doi.org/10.1016/j.jbc.2022.101706>

Canyang Niu¹, Xiaoying Sun^{1,2}, Fang Hu^{1,2}, Xiaowen Tang^{2,3,*}, and KeWei Wang^{1,2,*} 

From the ¹Department of Pharmacology, Qingdao University School of Pharmacy, Qingdao, China; ²Institute of Innovative Drugs, Qingdao University, Qingdao, China; ³Department of Medicinal Chemistry, Qingdao University School of Pharmacy, Qingdao, China

Edited by Mike Shipston

Transient receptor potential vanilloid 3 (TRPV3), robustly expressed in the skin, is a nonselective calcium-permeable cation channel activated by warm temperature, voltage, and certain chemicals. Natural monoterpene carvacrol from plant oregano is a known skin sensitizer or allergen that specifically activates TRPV3 channel. However, how carvacrol activates TRPV3 mechanistically remains to be understood. Here, we describe the molecular determinants for chemical activation of TRPV3 by the agonist carvacrol. Patch clamp recordings reveal that carvacrol activates TRPV3 in a concentration-dependent manner, with an EC₅₀ of 0.2 mM, by increasing the probability of single-channel open conformation. Molecular docking of carvacrol into cryo-EM structure of TRPV3 combined with site-directed mutagenesis further identified a unique binding pocket formed by the channel S2-S3 linker important for mediating this interaction. Within the binding pocket consisting of four residues (Ile505, Leu508, Arg509, and Asp512), we report that Leu508 is the most critical residue for the activation of TRPV3 by carvacrol, but not 2-APB, a widely used nonspecific agonist and TRP channel modulator. Our findings demonstrate a direct binding of carvacrol to TRPV3 by targeting the channel S2-S3 linker that serves as a critical domain for chemical-mediated activation of TRPV3. We also propose that carvacrol can function as a molecular tool in the design of novel specific TRPV3 modulators for the further understanding of TRPV3 channel pharmacology.

As a member of transient receptor potential vanilloid (TRPV) cation channel subfamily, the multimodal and nonselective calcium-permeable TRPV3 is robustly expressed in the skin and is activated by innocuous temperature at 31 to 33 °C, membrane potential, and chemical ligands (1–3). Accumulating evidence shows that TRPV3 channel is involved in a variety of physiological and pathological functions including skin inflammation, cutaneous pain, chronic itch, thermosensation, and hair growth (4–7). Genetic gain-of-function mutations of TRPV3 cause a rare congenital

disorder of Olmsted syndrome characterized by palmoplantar, periorificial keratoderma, alopecia, and severe itch (8–14), suggesting that TRPV3 may serve as a therapeutic target for pruritus and skin-related diseases.

TRPV3 forms a tetrameric channel complex with each subunit consisting of six transmembrane-spanning segments (S1-S6), a pore-forming loop between S5 and S6, and cytosolic amino- (N-) and carboxy- (C-) termini (15). The ion permeation pathway of TRPV3 is lined by the S6 helices and the extended portions of the pore loops, including selectivity filter, central cavity, and gates (16). The S6 methionine residues (M677) form the intracellular gate with their side chains organized as a hydrophobic seal facing toward the center of ion permeation pathway (17). Unlike the gating rearrangements in TRPV1 (18, 19) and TRPV6 (20), upon heat or agonist binding, both the outer pore and the intracellular gate alone with conformational changes propagate to the TRP helix and result in overall conformational changes in TRPV3, especially the S1-S4 domains and the intracellular skirt rotating around the pore domain and expelling the lipids (17). The S1-S4 domain structural rearrangements underline the distinct gating mechanism of TRPV3 function (17).

TRPV3 is activated by a variety of chemicals, including natural compounds such as camphor, carvacrol, thymol, synthesized 2-aminoethyl diphenylborinate (2-APB), and intracellular protons (21–23). As a widely used tool molecule, 2-APB not only activates TRPV3 or other members of TRPs such as TRPV1, TRPV2, TRPA1, and TRP melastatin 6 (TRPM6) (24–26) but also inhibits TRPM2, TRPM8, TRP canonical 4 (TRPC4), TRPC5, and TRPC6 channels (27–29). Chemical activation of TRPV3 is featured of different gating mechanisms. Electrophysiological characterizations confirm that two residues H426 in pre-S1 and R696 in the TRP helix are specifically required for TRPV3 sensitivity to 2-APB, but not camphor or voltage (23, 30, 31). Camphor also activates TRPV3 with an EC₅₀ about 6 mM, involving the S4-S5 linker for its binding (30, 32). Natural monoterpene carvacrol (5-Isopropyl-2-methylphenol) as a skin sensitizer is a major component of plant oregano and has been shown to activate

* For correspondence: KeWei Wang, wangkw@qdu.edu.cn; Xiaowen Tang, xwtang1219@qdu.edu.cn.

Molecular mechanism for TRPV3 activation by carvacrol

TRPV3 with an EC_{50} of 0.497 ± 0.07 mM (23, 30). Carvacrol also activates TRPA1 and causes the channel acute desensitization (23). Our previous investigations show that pharmacological activation of TRPV3 by carvacrol induces pruritus in mice, but not in TRPV3-KO mice (33, 34). In addition, TRPV3 inhibitor natural forsythoside B (FB) attenuates pruritus, and cytotoxicity of keratinocytes induces by carvacrol (35). However, how TRPV3 is activated by agonist carvacrol remains unknown. Understanding the molecular mechanism for specific activation of TRPV3 by carvacrol may lead to identification of more specific modulators for the study of TRPV3 pharmacology.

In this study, we investigated the molecular determinates underlying the chemical activation of TRPV3 by specific agonist carvacrol using combined approaches of electrophysiology, molecular docking, and site-directed mutagenesis. Our findings reveal that carvacrol binds to a key pocket formed by the S2-S3 linkers and leads to the activation of TRPV3 channels.

Results

Carvacrol increases TRPV3 single channel open probability

To demonstrate the direct action of carvacrol on TRPV3, we started recapitulating TRPV3 current activation in response to different concentrations of carvacrol. As shown in Figure 1A, carvacrol activated the whole-cell currents of WT TRPV3 channels in a concentration-dependent manner with an EC_{50} value of 215.0 ± 47.9 μ M. Further single-channel recordings at voltages ranging from -80 mV to $+80$ mV confirmed that carvacrol at 300 μ M also caused a voltage-dependent activation of TRPV3 single-channels with a unitary conductance of 182.0 ± 6.4 pS (Fig. 1B), similar to the commonly used agonist 2-APB (50 μ M) that also voltage-dependently activated TRPV3 single channels with a unitary conductance at 173.2 ± 5.3 pS (Fig. 1C).

To further characterize the effect of carvacrol on TRPV3 activation, we carried out the single-channel recordings in inside-out patch configuration. Carvacrol at 300 μ M or 50 μ M 2-APB as control increased TRPV3 single-channel open probability, whereas TRPV3 inhibitor FB reduced the agonist-induced single channel openings (Fig. 2, A and B). Further quantitative analysis showed that carvacrol led to an increase of P_o to 0.72 ± 0.05 and an open Freq to 59.21 ± 11.32 Hz as compared with the control, whereas FB at 50 μ M reduced the P_o to 0.12 ± 0.03 and open Freq to 21.78 ± 2.59 Hz, respectively (Fig. 2, C–F). Similarly, 2-APB at 50 μ M led to an increase of P_o to 0.77 ± 0.07 and an open Freq to 65.48 ± 12.31 Hz as compared with the control, whereas FB at 50 μ M reduced the P_o to 0.12 ± 0.08 and open Freq to 20.07 ± 1.77 Hz (Fig. 2, C–F). These observations demonstrate that carvacrol directly acts on TRPV3 at macroscopic and single-channel current levels.

Identification of S2-S3 linker domain critical to TRPV3 activation by carvacrol

To understand the interaction between carvacrol and TRPV3, we employed the molecular docking and analyzed the

top five of eight binding pockets from the prediction of binding affinity scores (Fig. 3, A and B and Table S1). The pocket 1 and 2 formed by four helices S1-S4 are located above the membrane and within the membrane, respectively (Fig. 3, C and D). The pocket 3 is located at the pre-S1 helix and the TRP helix domain (Fig. 3E). Pockets 1 to 3 are all involved in 2-APB-mediated activation of TRPV3 (17). The pocket 4 is formed between S1 helix and S4 helix (Fig. 3F), and the pocket 5 is formed by the S2-S3 linker (Fig. 3G).

Analyzing the binding mode from docking reveals distinct hydrogen bonds between the pocket residues and carvacrol (Fig. 3, C–G). Further energy decomposition indicates that those hydrogen bonds provide the most significant contributions to the ligand binding (Fig. S1, A–E). To test this notion, we carried out site-directed mutagenesis combined with current recordings. Mutating the key residues forming the hydrogen bond with carvacrol resulted in an ablation of carvacrol-mediated TRPV3 activation within the pocket 5, but not mutations in the pockets 1 to 4 that retained the channel activation by carvacrol, as compared to WT TRPV3 (Fig. 3, C–H). These results demonstrate that the pocket 5 formed by the S2-S3 linker is an important domain for carvacrol-mediated TRPV3 activation.

Molecular determinants for TRPV3 activation by carvacrol

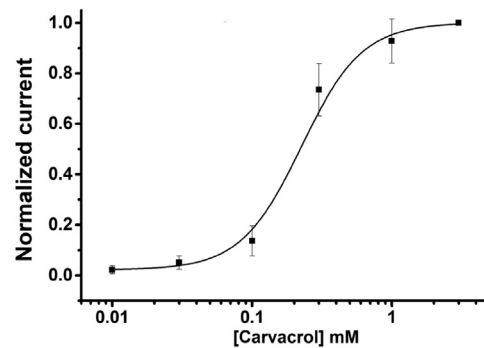
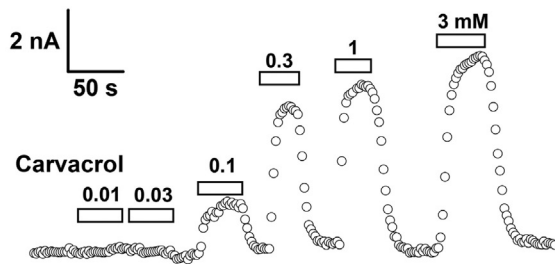
The chemical structure of carvacrol is featured of an isopropyl group with two methyl arms, a hydroxyl leg, a methyl tail, and the aromatic core (Fig. 4A). To further confirm the residue L508 in the pocket 5 critical for binding to the hydroxyl leg of carvacrol by forming the hydrogen bond (Fig. 4B), we mutated the residue L508 into different amino acids and analyzed the mutant channel sensitivity to carvacrol.

Molecular docking shows an orientation suitable for carvacrol with its hydroxyl leg and isopropyl arms nicely landing on two-sunken potholes of the pocket surface in WT TRPV3 (Fig. 4C), resulting in a stable hydrogen bond interaction with the main chain of residue L508. Whole-cell current or single-channel recordings of WT TRPV3 further confirmed that the channel was responsive to different concentrations of carvacrol or 2-APB at 50 μ M (Fig. 4, D and K). Virtual mutation of L508 to alanine (L508A) results in a loss of hydrogen bond interaction with the hydroxyl leg of carvacrol (Fig. 4E, left) and a reduction of one sunken pothole (Fig. 4E, right), thus weakening the hydrogen bond interaction between carvacrol and L508A. Whole-cell current or single-channel recordings of TRPV3 L508A mutant further confirmed the loss of the mutant channel activation by carvacrol, but not 2-APB that was still able to activate the mutant channel (Fig. 4, F and K). Similarly, mutating L508 to L508F altering the surface of the pocket also ablated TRPV3 activation by carvacrol, but not 2-APB (Fig. 4, G, H and K).

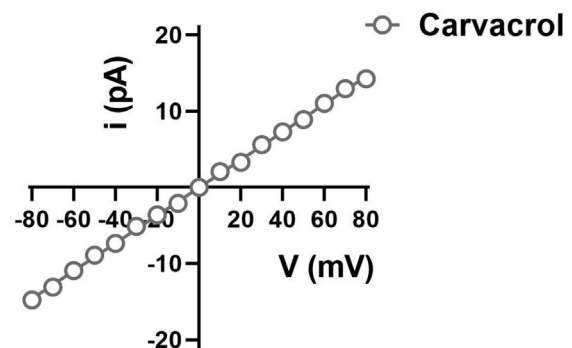
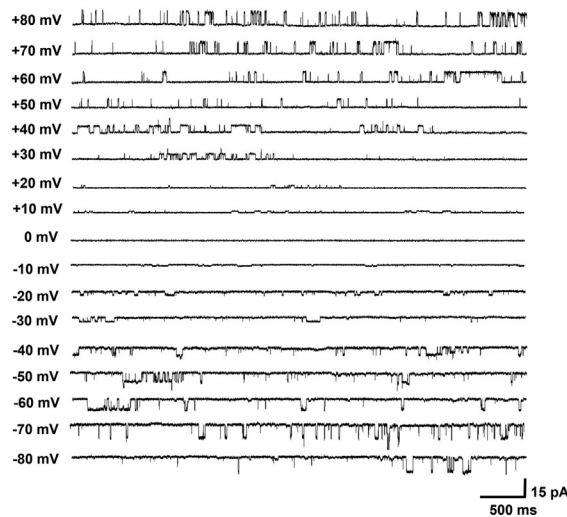
Interestingly, mutating L508 to a structurally similar valine (L508V) was also able to retain the channel activation of TRPV3 L508V mutant by carvacrol with its hydroxyl leg and the isopropyl arms falling on the two sunken potholes on the pocket surface as the ligand was still able to form the hydrogen

A

hTRPV3-WT



B



C

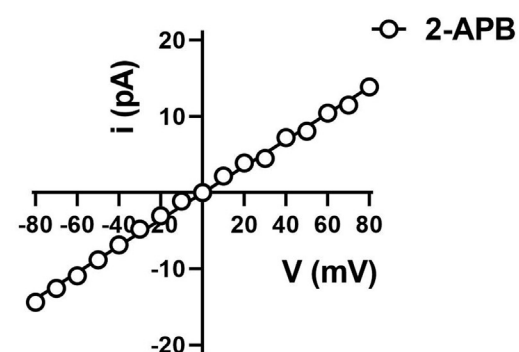
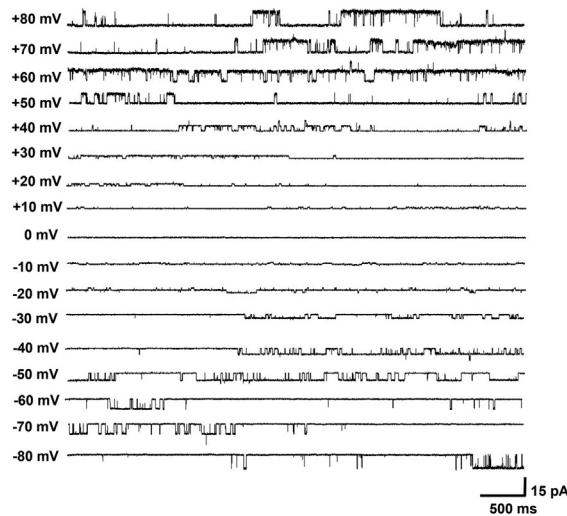


Figure 1. Dose- and voltage-dependent activation of TRPV3 channel currents by carvacrol and 2-APB. A, whole-cell patch-clamp recordings of TRPV3 currents in response to different concentrations of carvacrol ranging from 0.01 to 3.0 mM with an EC_{50} of $215.0 \pm 47.94 \mu\text{M}$ ($n = 6$). B, left panel, representative single-channel current (inside-out patches) traces induced by depolarizing potentials from -80 mV to $+80$ mV in the presence of carvacrol ($300 \mu\text{M}$); right panel, the I-V relationship of TRPV3 single-channel currents evoked by carvacrol (gray circles) with a unitary conductance of 182.0 ± 6.4 pS ($n = 4$) obtained by fitting a linear function. C, left panel, representative single-channel current (inside-out patches) traces in response to depolarizing potentials from -80 mV to $+80$ mV in the presence of 2-APB; right panel, the I-V relationship of TRPV3 single-channel currents in response to $50 \mu\text{M}$ 2-APB (black circles) with a unitary conductance of 173.2 ± 5.3 pS ($n = 4$) obtained by fitting a linear function. All statistical data are expressed as the mean \pm SD. 2-APB, 2-aminoethyl diphenylborinate; TRPV3, Transient receptor potential vanilloid 3.

Molecular mechanism for TRPV3 activation by carvacrol

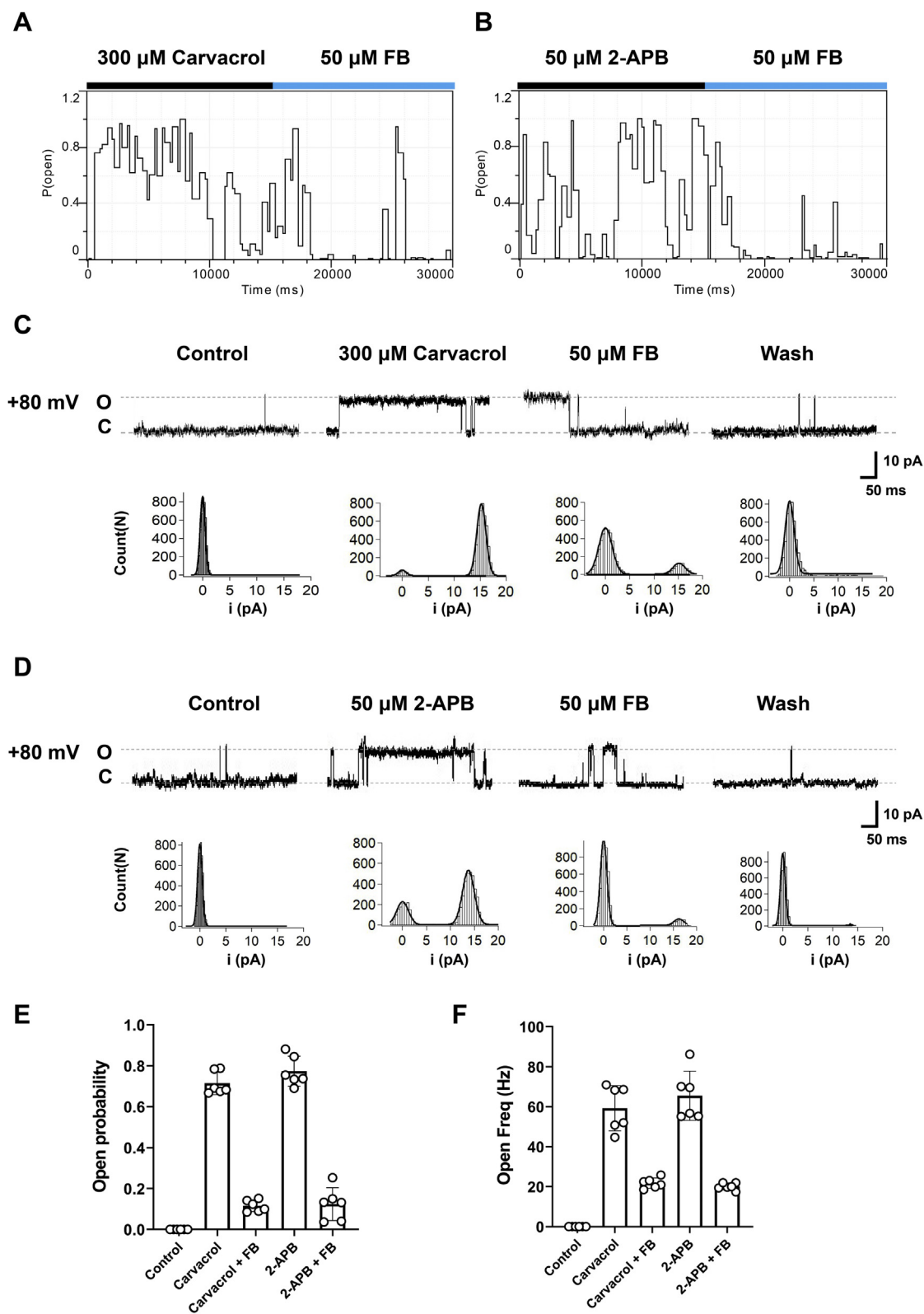


Figure 2. The increase of single TRPV3 channel open probability by carvacrol. *A* and *B*, plots of time course for P_o of single TRPV3 channels recorded from inside-out macropatches (at +80 mV) in the presence of 300 μM carvacrol or 50 μM 2-APB before the addition of 50 μM TRPV3 blocker forsythoside B (FB). *C* and *D*, representative single-channel current traces recorded at +80 mV before and after the addition of 300 μM carvacrol (*C*) or 50 μM of 2-APB (*D*) with or without 50 μM TRPV3 blocker FB before washout. All-point amplitude histograms of single-channel currents were shown in their lower panels. Letters O and C indicate channel open state and closed state, respectively. *E* and *F*, summary for effects of carvacrol and 2-APB on TRPV3 single-channel open probability (left) and open frequency (Freq) (right) in the presence or absence of FB. All statistical data are expressed as the mean \pm SD. 2-APB, 2-aminoethyl diphenylborinate; P_o , open probability; TRPV3, Transient receptor potential vanilloid 3.

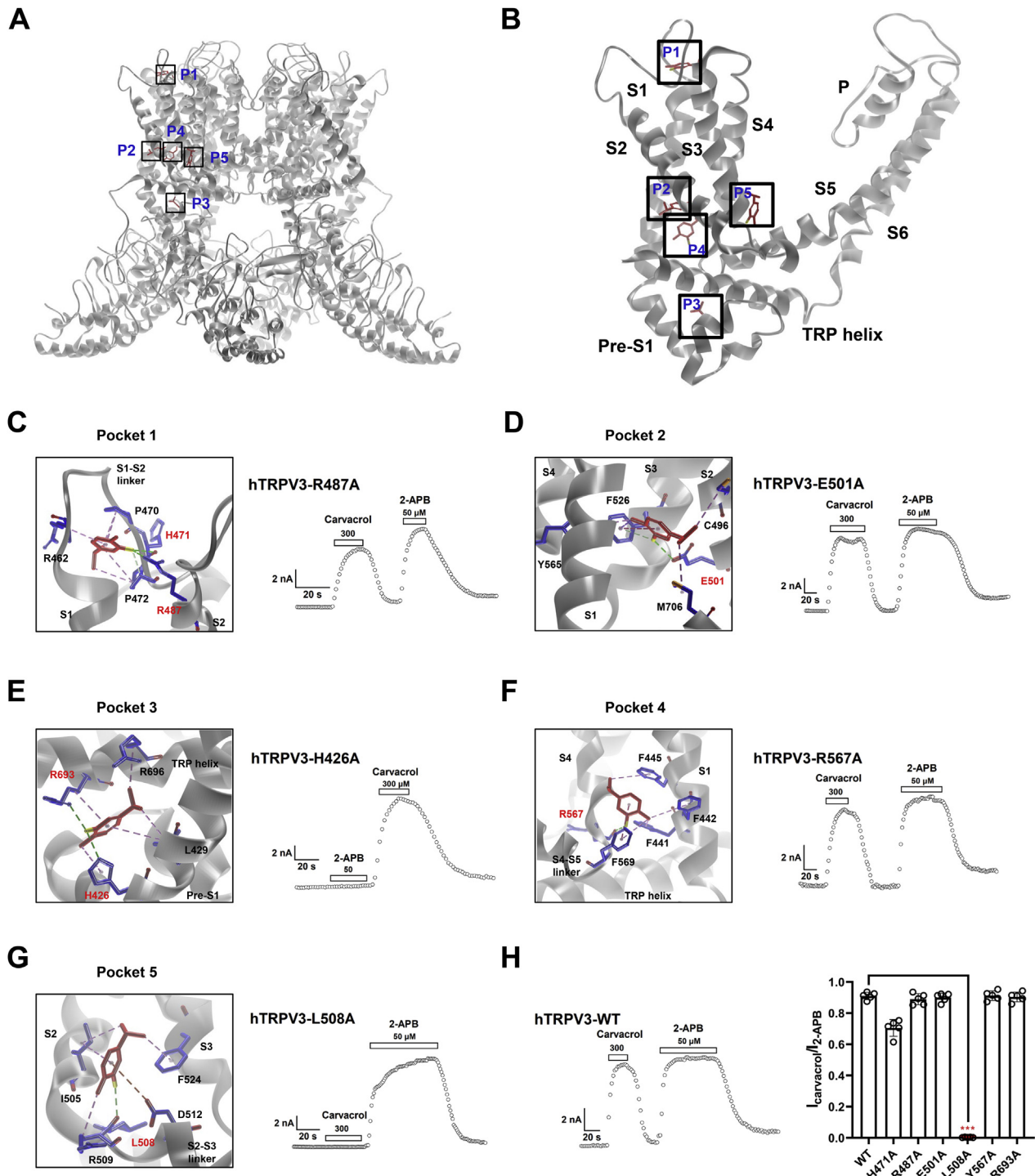


Figure 3. Identification of a binding pocket formed by S2-S3 linker critical for interaction between carvacrol and TRPV3. *A*, an overview of putative five pockets for carvacrol binding to TRPV3 structure from docking. *B*, a representative view showing the binding of carvacrol to one subunit of TRPV3 in the five binding pockets (P1–5). *C*, *left panel*, carvacrol in the binding pocket 1 with putative interaction residues; *right panel*, representative TRPV3-R487A whole-cell currents in response to 300 μ M carvacrol or 50 μ M 2-APB. *D*, *left panel*, carvacrol in the binding pocket 2 with putative interaction residues; *right panel*, representative TRPV3-E501A whole-cell currents in response to 300 μ M carvacrol and 50 μ M 2-APB. *E*, *left panel*, carvacrol in the binding pocket 3 with putative interaction residues; *right panel*, representative TRPV3-H426A whole-cell currents in response to 300 μ M carvacrol or 50 μ M 2-APB. *F*, *left panel*, carvacrol in the binding pocket 4 with putative interaction residues; *right panel*, representative TRPV3-R567A whole-cell currents in response to 300 μ M carvacrol or 50 μ M 2-APB. *G*, *left panel*, carvacrol in the binding pocket 5 with putative interaction residues; *right panel*, representative TRPV3-L508A whole-cell currents in response to 300 μ M carvacrol and 50 μ M 2-APB. *H*, *left panel*, representative WT TRPV3 whole-cell currents in response to 300 μ M carvacrol or 50 μ M 2-APB; *right panel*, a summary of normalized currents for the comparison of activation of WT TRPV3 and mutant channels by carvacrol ($n = 5$, $***p < 0.001$). Carvacrol in a schematic structure is shown in red and molecular residues involved are shown in blue. Key amino acids are labeled in red font. All data are expressed as the mean \pm SD. 2-APB, 2-aminoethyl diphenylborinate; TRPV3, Transient receptor potential vanilloid 3.

Molecular mechanism for TRPV3 activation by carvacrol

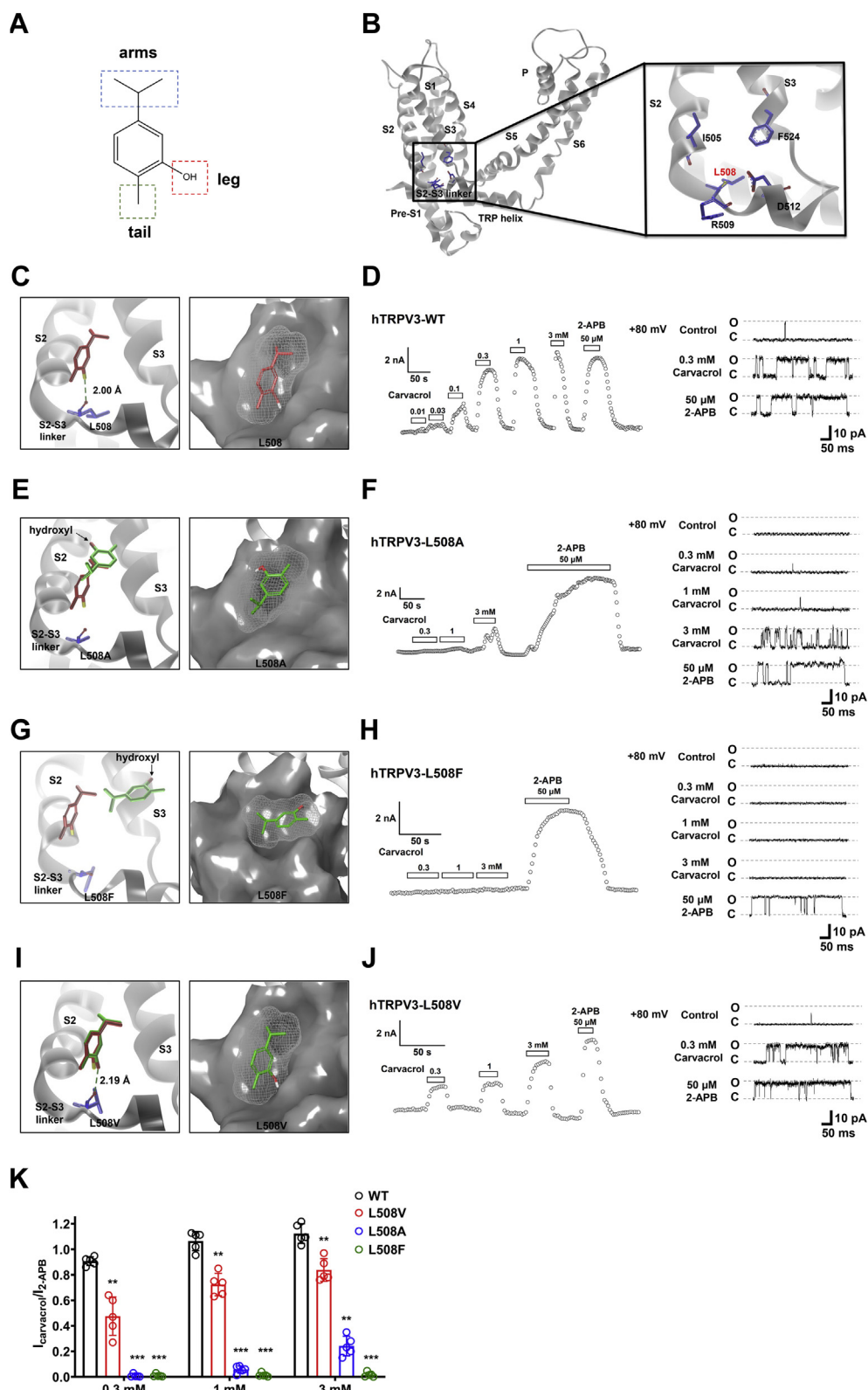


Figure 4. Confirmation of residue L508 in the pocket 5 critical for carvacrol-mediated activation of TRPV3. *A*, the chemical structure of carvacrol featuring the moieties of an isopropyl group with two-methyl arms, a hydroxyl leg, and a methyl tail. *B*, an overview of one subunit and its zoom-in view of the binding pocket formed by residues L505, L508, R509, D512, and F524. *C*, *left panel*, docking predicts a hydrogen bond between the hydroxyl leg of carvacrol (in red) and the residue L508 (in blue); *right panel*, a representative surface binding posture of carvacrol (in red) in the pocket of TRPV3 S2-S3. *D*, *left panel*, concentration-dependent activation of WT TRPV3 currents by carvacrol in whole-cell recordings and single-channel current traces (*right panel*) ($n = 5$). *E*, *left panel*, virtual mutation of TRPV3-L508A in docking with carvacrol (in green) altering the binding mode in the pocket; *right panel*, a representative surface binding posture of carvacrol (in green) in the pocket. *F*, representative whole-cell current recordings of TRPV3-L508A (*left panel*) and single-channel current traces (*right panel*) in response to different concentrations (0.3–3.0 mM) of carvacrol or 50 μM 2-APB ($n = 5$). *G*, *left panel*, virtual mutation of TRPV3-L508F in docking with carvacrol (in green) altering the binding mode in the pocket; *right panel*, a representative surface binding posture of carvacrol

bond with L508V (although increased by 0.19 Å) (Fig. 4, I–K). Collectively, these results show that the formation of the hydrogen bond between carvacrol and L508 is critical for chemical activation of TRPV3.

Relationship of chemical structure of carvacrol and its activities

Carvacrol stands on residue L508 with its hydroxyl leg, while its isopropyl arms seize the two neighboring residues I505 and F524 with its methyl tail binding to residue R509. In addition, a π -anion interaction between the aromatic core and residue D512 is also involved in maintaining the binding stability (Fig. 4, A and B). The isopropyl arms exhibit alkyl-alkyl & π -alkyl interactions with residue I505 (Fig. 5A) and a π -alkyl interaction with F524 (Fig. S2A). Mutating I505 to I505A led to a significant loss of the channel sensitivity to carvacrol that only caused a weak activation of TRPV3 I505A at high concentration of 3 mM, as compared with WT TRPV3 or an intact activation of TRPV3 by 50 μ M 2-APB (Fig. 5B). Mutating F524 to F524A resulted in a loss of surface expression and reduced sensitivity to 50 μ M 2-APB (Fig. S2B).

The methyl tail of carvacrol interacts with the residue R509 through alkyl-alkyl interaction (Fig. 5C) and the point mutation R509A also decreased the channel sensitivity to carvacrol at both macroscopic current and single-channel current levels (Fig. 5D). In addition, the aromatic core of carvacrol binds to the residue D512 through π -anion interaction (Fig. 5E), and the mutation D512A also decreased the sensitivity to carvacrol (Fig. 5F). In comparison with the activation of WT TRPV3 by carvacrol with an EC_{50} at 0.18 ± 0.03 mM, mutating I505A, R509A, and D512A resulted in the right shift of the channel activation to higher concentration for over 10-fold with EC_{50} values of 3.51 ± 0.44 mM, 2.93 ± 0.11 mM, and 3.21 ± 0.48 mM, respectively (Fig. 5, G and H). These results demonstrate that the L508 together with three residues I505, R509, and D512 within the domain of S2-S3 are critical for carvacrol-mediated activation of TRPV3 channel.

Discussion

The goal of this study was to investigate the molecular mechanism of action for natural carvacrol that specifically activates TRPV3 in comparison with a commonly and widely used agonist 2-APB. Using a combination of patch-clamp recordings, molecular docking analysis, and site-directed mutagenesis, we find that the agonist carvacrol activates TRPV3 currents through a direct action on the target at the single channel levels. We also identify a binding pocket primarily

formed by four key amino acids I505, L508, R509, and D512 within the S2-S3 linker that confers the chemical activation of TRPV3 by carvacrol.

Multimodal TRPV3 exhibits different unitary conductances in response to chemical or heat stimulation (36–38). Heat at 42 °C activates TRPV3 with a unitary conductance at 146 ± 7 pS (36, 37). Chemical activation of TRPV3 by 2-APB in the presence or absence of TRPV3 inhibitor dyclonine also reveals a different unitary conductance of 179.2 ± 5.5 pS and 163.6 ± 6.4 pS, respectively (38). In this study, our single-channel recordings of TRPV3 activation by carvacrol and 2-APB at voltages ranging from -80 mV to $+80$ mV show a unitary conductance of 182.0 ± 6.4 pS and 173.2 ± 5.3 pS, respectively.

The cryo-EM structures of TRPV3 reveal that agonist 2-APB binds to a pocket formed by the top of S1-S4 domains (17), and the interface between S1-S4 and the pore domain is rearranged, causing the move of S5 and S6 away from the pore with an overall dramatic change of TRPV3 conformation (17). In this study, we tested five potential binding pockets from virtual predictions and identified the residues I505, L508, R509, and D512 within TRPV3 S2-S3 linker domain that confers carvacrol-mediated channel activation. Carvacrol interacts with a key residue L508 in the S2-S3 linker, likely causing a conformational reorganization before channel opening.

The S2-S3 linker has been shown to play an important role in multimodal gating of TRPV1 that shares about 43% sequence similarity with TRPV3 (39–41). Thermal activation of TRPV1 channel is involved in several linker domains such as the membrane proximal domain loop, the S2-S3 linker, and the S4-S5 linker, all contributing to the allosteric couplings underlying either heat or agonist-mediated channel activation (42–45). A recent investigation shows that heat-induced transformations of TRPV3 are accompanied by a massive conformational wave involving structural changes of the secondary structure and positioning changing of the S2-S3 linker and the N and C termini for the channel opening and temperature sensing (37). For chemical activation of TRPV3, we find that L508, one of the important residues within the S2-S3 linker, plays a critical role in chemical activation of TRPV3 by carvacrol with its both hydroxyl leg and methyl tail serving as two pivotal pillars for binding and stabilizing the channel open conformation. In addition, the isopropyl arms of carvacrol cause the motion of S2-S3 domain by grasping I505 in the S2 and F524 in the S3 in combination with the π -anion interaction between the aromatic core and the residue D512. Such a mechanical force or wave can lead to conformational changes in a domino-like propagation, thus resulting in the pore widening (Fig. 6).

(in green) in the pocket. H, representative whole-cell current recordings of TRPV3-L508F (left panel) and single-channel current traces (right panel) in response to different concentrations (0.3–3.0 mM) of carvacrol or 50 μ M 2-APB ($n = 5$). I, left panel, virtual mutation of TRPV3-L508V in docking with carvacrol (in green), altering the binding mode in the pocket; right panel, a representative surface binding posture of carvacrol (in green) in the pocket. J, left panel, concentration-dependent activation of TRPV3-L508V currents by carvacrol in whole-cell recordings and single-channel current traces (right panel) ($n = 5$). K, a summary of normalized currents for concentration-dependent activation of WT TRPV3 and its mutant channels by carvacrol (0.3–3 mM) ($n = 5$). The dominant conformations of carvacrol in WT TRPV3 and mutants are shown in red sticks and green sticks, respectively. Gray surface area indicates the density of TRPV3 and light gray mesh shows the density of carvacrol. All data are expressed as the mean \pm SD, ** $p < 0.01$, *** $p < 0.001$, by unpaired t test. 2-APB, 2-aminoethyl diphenylborinate; TRPV3, Transient receptor potential vanilloid 3.

Molecular mechanism for TRPV3 activation by carvacrol

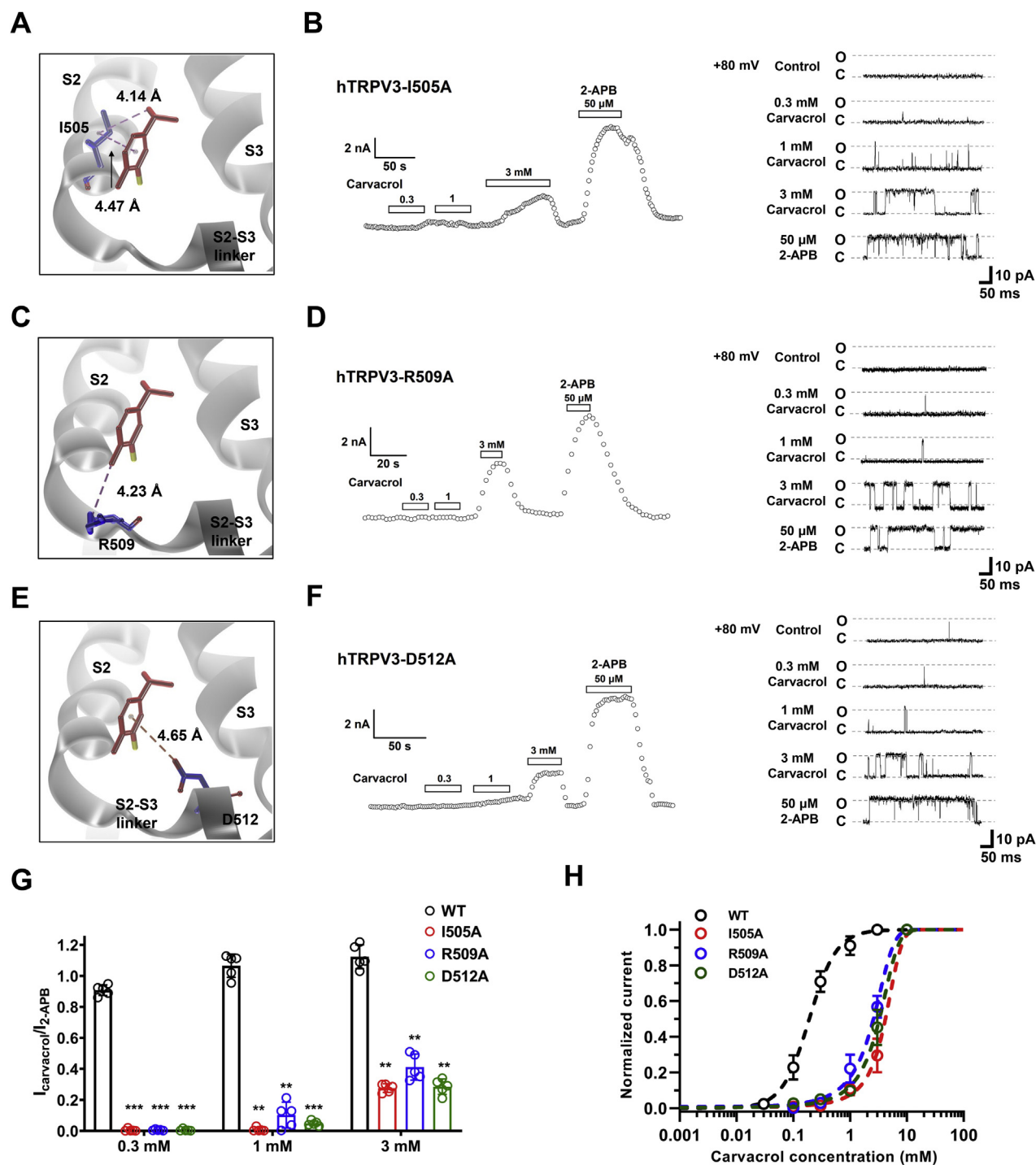


Figure 5. Molecular determinants in the binding pocket of S2-S3 critical for activation of TRPV3 by carvacrol. *A*, molecular docking showing alkyl-alkyl & π -alkyl interactions between isopropyl arms and aromatic core of carvacrol and residue I505. *B*, representative whole-cell current recordings of TRPV3-I505A (left panel) and single-channel current traces (right panel) in response to different concentrations (0.3–3.0 mM) of carvacrol or 50 μ M 2-APB ($n = 5$). *C*, molecular docking showing alkyl-alkyl interaction between methyl tail of carvacrol and residue R509. *D*, representative whole-cell current recordings of TRPV3-R509A (left panel) and single-channel current traces (right panel) in response to different concentrations (0.3–3.0 mM) of carvacrol or 50 μ M 2-APB ($n = 5$). *E*, molecular docking showing π -anion interaction between carvacrol and residue D512. *F*, representative whole-cell current recordings of TRPV3-D512A (left panel) and single-channel current traces (right panel) in response to different concentrations (0.3–3.0 mM) of carvacrol or 50 μ M 2-APB ($n = 5$). *G*, a summary of normalized currents for concentration-dependent activation of WT TRPV3 and mutant channels by carvacrol (0.3–3 mM) ($n = 5$). *H*, a summary for the comparison of concentration–response curves of activation of WT and mutant TRPV3 currents by carvacrol ($n = 5$). Dotted lines are fits to Hill equation, yielding WT TRPV3 with EC_{50} of 0.18 ± 0.03 mM ($n = 5$). Mutations I505A, R509A, and D512A showed EC_{50} values with 3.51 ± 0.44 mM, 2.93 ± 0.11 mM, and 3.21 ± 0.48 mM, respectively ($n = 5$). All data are expressed as the mean \pm SD, ** $p < 0.01$, *** $p < 0.001$, by unpaired *t* test. 2-APB, 2-aminoethyl diphenylborinate; TRPV3, Transient receptor potential vanilloid 3.

Molecular mechanism for TRPV3 activation by carvacrol

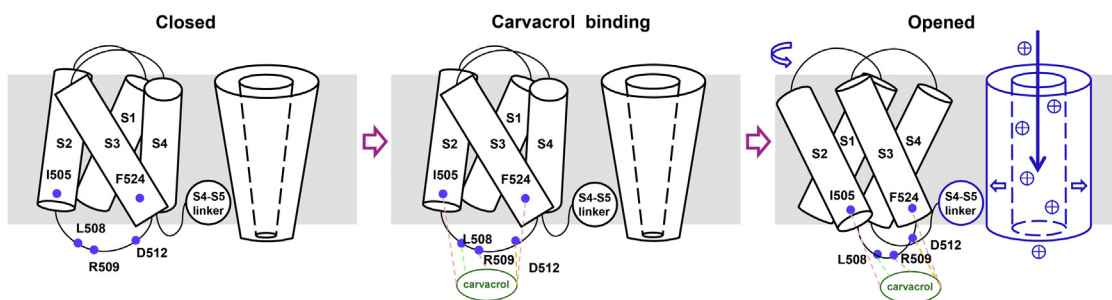


Figure 6. Proposed model for binding of S2-S3 and activation of TRPV3 channel by carvacrol. Carvacrol-mediated activation of TRPV3 channels involves the ligand binding and channel opening. Carvacrol binding to S2-S3 linker leads to conformational changes that propagate from the channel periphery to the channel pore opening. TRPV3, Transient receptor potential vanilloid 3.

The hydroxyl group of carvacrol as “a leg” is essential for the formation of the hydrogen bond critical for TRPV3 activation. In comparison with carvacrol, the structure-derivative monoterpene agonists p-Xylenol without the isopropyl arms or p-Cymene without the hydroxyl leg can only induce either small or negligible TRPV3 currents (30).

In conclusion, our findings unravel a direct action of natural carvacrol on TRPV3 channels through a binding pocket formed by the S2-S3 linker. The identification of the agonist carvacrol-binding pocket in TRPV3 S2-S3 linker not only helps understand the pharmacological gating of the channel but also serves as a target for further synthesis of novel TRPV3 modulators with improved specificity and potency.

Experimental procedures

Molecular biology and cell transfection

All mutations were constructed on human TRPV3 (accession number NM_145068.4) and confirmed by DNA sequencing. Primers used to generate point mutations are summarized in Table S2. Point mutations were made using Fast Mutagenesis Kit V2 (C214-02, Vazyme Biotech Co, Ltd). Human embryonic kidney 293 (HEK293) cells were cultured in Dulbecco’s modified Eagle’s medium (DMEM) supplemented with 10% fetal bovine serum and kept in an incubator at 37 °C in an atmosphere with 95% O₂ and 5% CO₂. HEK293 cells were plated onto glass coverslips 24 h before cDNA transfection. Transient transfection was conducted by adding 1.6 µg human TRPV3 cDNA in pIRES2-enhanced green fluorescent protein vector and 3.2 µl Lipofectamine 2000 (11668019, Invitrogen) into opti-MEM before kept at room temperature for 20 min. The experiments took place 12 to 24 h after transfection.

Chemicals

Carvacrol and 2-APB were purchased from Sigma-Aldrich Corp. Natural compound FB were obtained from Tauto Biotech Corporation, Ltd, and camphor were obtained from TargetMol and stored at -20 °C daily. Stock solutions of carvacrol (300 mM), 2-APB (1 M), FB (100 mM), and camphor (1 M) were prepared in dimethyl sulfoxide.

Whole-cell patch clamp recordings

For whole-cell recordings, the borosilicate glass pipette was pulled and fire-polished to a resistance of 3 to 4 MΩ using a

DMZDMZ-Universal puller (Zeitz-Instruments, GmbH). The bath solution contained (in mM) the following: NaCl 130, KCl 5, CaCl₂ 2, MgCl₂ 1, glucose 30, Hepes–NaOH 25, pH 7.3. The pipette solution consisted (in mM) the following: CsCl 140, MgCl₂ 4, EGTA 10, Hepes–CsOH 10, pH 7.3. Transient receptor potential vanilloid 3 channel currents were recorded in transfected HEK293 cells held at 0 mV in response to a voltage ramp from -100 mV to +100 mV for 500 ms, and the current was analyzed at ± 80 mV. All patch clamp recordings were performed at room temperature (22 ± 2 °C).

Inside-out single channel recordings

Patch-clamp recordings were carried out using a HEKA EPC10 amplifier powered by PatchMaster software (HEKA, Instrument Inc). Patch pipettes were prepared using borosilicate glass and fire-polished to a resistance of 5 to 6 MΩ using a DMZDMZ-Universal puller (Zeitz-Instruments, GmbH). The recording solution (in mM) containing NaCl 130, glucose 10, EDTA 0.2, and Hepes 3 (pH 7.2) was used in both bath and pipette. Membrane potential was clamped at +80 mV, and current was sampled at 10 kHz and filtered at 2 kHz. All patch clamp recordings were performed at room temperature (22 ± 2 °C).

Molecular docking

The interaction between carvacrol and TRPV3 2-APB-bound cryo-EM structure (PDB ID code: 6DVY) was analyzed using molecular docking approach. The 3D structure of carvacrol was derived from the PubChem database. Docking calculations were completed using the AutoDock 4.2 program (46). The Lamarckian genetic algorithm was used in the docking simulation for ligand conformational searching according to the standard protocol. After docking the pose score, the lowest binding energy was chosen to visualize ligand–protein interactions using MOE 2020. Protein builder in MOE 2020 was used for amino acid mutation, and energy minimization is used to obtain the dominant configuration.

Data analysis

Data were analyzed offline with Igor Pro (Wave-metrics), and GraphPad Prism 8.0, Clampfit 10.7 (Molecular Devices) and Origin 8.6 software (OriginLab) were used to analyze the

Molecular mechanism for TRPV3 activation by carvacrol

data. EC_{50} values were determined by fitting Hill equation to concentration–response relationships. Unless stated otherwise, all data are expressed as the mean \pm SD, and statistical comparison for experimental data between two groups was conducted using unpaired Student's *t* test. A value of $p < 0.05$ is considered to be statistically significant.

Data availability

All data are contained within the article.

Supporting information—This article contains supporting information (37).

Acknowledgments—This work was supported by National Natural Science Foundation of China (81903734 and 81973299) and the Ministry of Science and Technology of China (2018ZX09711001-004-006).

Author contributions—C. N., F. H., X. T., and K. W. methodology; C. N. validation; C. N., X. S., F. H., and X. T. formal analysis; C. N., X. S., F. H., X. T., and K. W. writing—original draft; C. N. visualization; X. T. and K. W. conceptualization; K. W. resources; C. N., X. S., F. H., X. T., and K. W. writing—review and editing; K. W. supervision; K. W. project administration; K. W. funding acquisition; C. N. investigation.

Conflict of interest—The authors declare no conflicts of interest in this study.

Abbreviations—The abbreviations used are: 2-APB, 2-aminoethoxydiphenyl borate; FB, forsythoside B; HEK293, human embryonic kidney 293; TRP, transient receptor potential; TRPC, TRP canonical; TRPM, TRP melastatin; TRPV, TRP vanilloid.

References

1. Peier, A. M., Reeve, A. J., Andersson, D. A., Moqrich, A., Earley, T. J., Hergarden, A. C., Story, G. M., Colley, S., Hogenesch, J. B., McIntyre, P., Bevan, S., and Patapoutian, A. (2002) A heat-sensitive TRP channel expressed in keratinocytes. *Science* **296**, 2046–2049
2. Smith, G. D., Gunthorpe, M. J., Kelsell, R. E., Hayes, P. D., Reilly, P., Facer, P., Wright, J. E., Jerman, J. C., Walhin, J. P., Ooi, L., Egerton, J., Charles, K. J., Smart, D., Randall, A. D., Anand, P., *et al.* (2002) TRPV3 is a temperature-sensitive vanilloid receptor-like protein. *Nature* **418**, 186–190
3. Xu, H., Ramsey, I. S., Kotecha, S. A., Moran, M. M., Chong, J. A., Lawson, D., Ge, P., Lilly, J., Silos-Santiago, I., Xie, Y., DiStefano, P. S., Curtis, R., and Clapham, D. E. (2002) TRPV3 is a calcium-permeable temperature-sensitive cation channel. *Nature* **418**, 181–186
4. Asakawa, M., Yoshioka, T., Matsutani, T., Hikita, I., Suzuki, M., Oshima, I., Tsukahara, K., Arimura, A., Horikawa, T., Hirasawa, T., and Sakata, T. (2006) Association of a mutation in TRPV3 with defective hair growth in rodents. *J. Invest. Dermatol.* **126**, 2664–2672
5. Imura, K., Yoshioka, T., Hikita, I., Tsukahara, K., Hirasawa, T., Higashino, K., Gahara, Y., Arimura, A., and Sakata, T. (2007) Influence of TRPV3 mutation on hair growth cycle in mice. *Biochem. Biophys. Res. Commun.* **363**, 479–483
6. Yoshioka, T., Imura, K., Asakawa, M., Suzuki, M., Oshima, I., Hirasawa, T., Sakata, T., Horikawa, T., and Arimura, A. (2009) Impact of the Gly573Ser substitution in TRPV3 on the development of allergic and pruritic dermatitis in mice. *J. Invest. Dermatol.* **129**, 714–722
7. Moqrich, A., Hwang, S. W., Earley, T. J., Petrus, M. J., Murray, A. N., Spencer, K. S., Andahazy, M., Story, G. M., and Patapoutian, A. (2005) Impaired thermosensation in mice lacking TRPV3, a heat and camphor sensor in the skin. *Science* **307**, 1468–1472
8. Lai-Cheong, J. E., Sethuraman, G., Ramam, M., Stone, K., Simpson, M. A., and McGrath, J. A. (2012) Recurrent heterozygous missense mutation, p. Gly573Ser, in the TRPV3 gene in an Indian boy with sporadic Olmsted syndrome. *Br. J. Dermatol.* **167**, 440–442
9. Lin, Z., Chen, Q., Lee, M., Cao, X., Zhang, J., Ma, D., Chen, L., Hu, X., Wang, H., Wang, X., Zhang, P., Liu, X., Guan, L., Tang, Y., Yang, H., *et al.* (2012) Exome sequencing reveals mutations in TRPV3 as a cause of Olmsted syndrome. *Am. J. Hum. Genet.* **90**, 558–564
10. Danso-Abeam, D., Zhang, J., Dooley, J., Staats, K. A., Van Eyck, L., Van Brussel, T., Zaman, S., Hauben, E., Van de Velde, M., Morren, M. A., Renard, M., Van Geet, C., Schaballie, H., Lambrechts, D., Tao, J., *et al.* (2013) Olmsted syndrome: Exploration of the immunological phenotype. *Orphanet J. Rare Dis.* **8**, 79
11. Duchatelet, S., Pruvost, S., de Veer, S., Fraitag, S., Nitschke, P., Bole-Feysot, C., Bodemer, C., and Hovnanian, A. (2014) A new TRPV3 missense mutation in a patient with Olmsted syndrome and erythromelalgia. *JAMA Dermatol.* **150**, 303–306
12. Eytan, O., Fuchs-Telem, D., Mevorach, B., Indelman, M., Bergman, R., Sarig, O., Goldberg, I., Adir, N., and Sprecher, E. (2014) Olmsted syndrome caused by a homozygous recessive mutation in TRPV3. *J. Invest. Dermatol.* **134**, 1752–1754
13. He, Y., Zeng, K., Zhang, X., Chen, Q., Wu, J., Li, H., Zhou, Y., Glusman, G., Roach, J., Etheridge, A., Qing, S., Tian, Q., Lee, I., Tian, X., Wang, X., *et al.* (2014) A gain-of-function mutation in TRPV3 causes focal palmoplantar keratoderma in a Chinese family. *J. Invest. Dermatol.* **135**, 907–909
14. Kariminejad, A., Barzegar, M., Abdollahimajid, F., Pramanik, R., and McGrath, J. A. (2014) Olmsted syndrome in an Iranian boy with a new de novo mutation in TRPV3. *Clin. Exp. Dermatol.* **39**, 492–495
15. Shioya, T., Sato, K., Sano, M., and Watanabe, H. (2008) Transient receptor potential (TRP) channel and cough. *Nihon Yakurigaku Zasshi* **131**, 417–422
16. Zubcevic, L., Herzik, M. A., Wu, M., Borschel, W. F., Hirschi, M., Song, A. S., Lander, G. C., and Lee, S.-Y. (2018) Conformational ensemble of the human TRPV3 ion channel. *Nat. Commun.* **9**, 4773
17. Singh, A. K., McGoldrick, L. L., and Sobolevsky, A. I. (2018) Structure and gating mechanism of the transient receptor potential channel TRPV3. *Nat. Struct. Mol. Biol.* **25**, 805–813
18. Liao, M., Cao, E., Julius, D., and Cheng, Y. (2013) Structure of the TRPV1 ion channel determined by electron cryo-microscopy. *Nature* **504**, 107–112
19. Gao, Y., Cao, E., Julius, D., and Cheng, Y. (2016) TRPV1 structures in nanodiscs reveal mechanisms of ligand and lipid action. *Nature* **534**, 347–351
20. McGoldrick, L. L., Singh, A. K., Saotome, K., Yelshanskaya, M. V., Twomey, E. C., Grassucci, R. A., and Sobolevsky, A. I. (2018) Opening of the human epithelial calcium channel TRPV6. *Nature* **553**, 233–237
21. Cao, X., Yang, F., Zheng, J., and Wang, K. (2012) Intracellular proton-mediated activation of TRPV3 channels accounts for the exfoliation effect of α -hydroxyl acids on keratinocytes. *J. Biol. Chem.* **287**, 25905–25916
22. Chung, M. K., Lee, H., Mizuno, A., Suzuki, M., and Caterina, M. J. (2004) 2-Aminoethoxydiphenyl borate activates and sensitizes the heat-gated ion channel TRPV3. *J. Neurosci.* **24**, 5177–5182
23. Xu, H., Delling, M., Jun, J. C., and Clapham, D. E. (2006) Oregano, thyme and clove-derived flavors and skin sensitizers activate specific TRP channels. *Nat. Neurosci.* **9**, 628–635
24. Hu, H. Z., Gu, Q., Wang, C., Colton, C. K., Tang, J., Kinoshita-Kawada, M., Lee, L. Y., Wood, J. D., and Zhu, M. X. (2004) 2-Aminoethoxydiphenyl borate is a common activator of TRPV1, TRPV2, and TRPV3. *J. Biol. Chem.* **279**, 35741–35748
25. Hinman, A., Chuang, H. H., Bautista, D. M., and Julius, D. (2006) TRP channel activation by reversible covalent modification. *Proc. Natl. Acad. Sci. U. S. A.* **103**, 19564–19568

26. Clapham, D. E. (2007) SnapShot: Mammalian TRP channels. *Cell* **129**, 220
27. Lievreumont, J. P., Bird, G. S., and Putney, J. W., Jr. (2005) Mechanism of inhibition of TRPC cation channels by 2-aminoethoxydiphenylborane. *Mol. Pharmacol.* **68**, 758–762
28. Togashi, K., Inada, H., and Tominaga, M. (2008) Inhibition of the transient receptor potential cation channel TRPM2 by 2-aminoethoxydiphenyl borate (2-APB). *Br. J. Pharmacol.* **153**, 1324–1330
29. Kuhn, F. J. P., Mathis, W., Cornelia, K., Hoffmann, D. C., and Luckhoff, A. (2017) Modulation of activation and inactivation by Ca²⁺ and 2-APB in the pore of an archetypal TRPM channel from *Nematostella vectensis*. *Sci. Rep.* **7**, 7245
30. Vogt-Eisele, A. K., Weber, K., Sherkheli, M. A., Vielhaber, G., Panten, J., Gisselmann, G., and Hatt, H. (2007) Monoterpenoid agonists of TRPV3. *Br. J. Pharmacol.* **151**, 530–540
31. Hu, H., Grandl, J., Bandell, M., Petrus, M., and Patapoutian, A. (2009) Two amino acid residues determine 2-APB sensitivity of the ion channels TRPV3 and TRPV4. *Proc. Natl. Acad. Sci. U. S. A.* **106**, 1626–1631
32. Nguyen, T. H. D., Itoh, S. G., Okumura, H., and Tominaga, M. (2021) Structural basis for promiscuous action of monoterpenes on TRP channels. *Commun. Biol.* **4**, 293
33. Cui, T. T., Wang, G. X., Wei, N. N., and Wang, K. (2018) A pivotal role for the activation of TRPV3 channel in itch sensations induced by the natural skin sensitizer carvacrol. *Acta Pharmacol. Sin.* **39**, 331–335
34. Qu, Y., Wang, G., Sun, X., and Wang, K. (2019) Inhibition of the warm temperature-activated Ca²⁺-permeable transient receptor potential vanilloid TRPV3 channel attenuates atopic dermatitis. *Mol. Pharmacol.* **96**, 393–400
35. Zhang, H., Sun, X., Qi, H., Ma, Q., Zhou, Q., Wang, W., and Wang, K. (2019) Pharmacological inhibition of the temperature-sensitive and Ca²⁺-permeable transient receptor potential vanilloid TRPV3 channel by natural forsythoside B attenuates pruritus and cytotoxicity of keratinocytes. *J. Pharmacol. Exp. Ther.* **368**, 21–31
36. Singh, A. K., McGoldrick, L. L., Demirkhanyan, L., Leslie, M., Zakharian, E., and Sobolevsky, A. I. (2019) Structural basis of temperature sensation by the TRP channel TRPV3. *Nat. Struct. Mol. Biol.* **26**, 994–998
37. Nadezhdin, K. D., Neuberger, A., Trofimov, Y. A., Krylov, N. A., Sinica, V., Kupko, N., Vlachova, V., Zakharian, E., Efremov, R. G., and Sobolevsky, A. I. (2021) Structural mechanism of heat-induced opening of a temperature-sensitive TRP channel. *Nat. Struct. Mol. Biol.* **28**, 564–572
38. Liu, Q., Wang, J., Wei, X., Hu, J., Ping, C., Gao, Y., Xie, C., Wang, P., Cao, P., Cao, Z., Yu, Y., Li, D., and Yao, J. (2021) Therapeutic inhibition of keratinocyte TRPV3 sensory channel by local anesthetic dyclonine. *Elife* **10**, e68128
39. Clapham, D. E. (2003) TRP channels as cellular sensors. *Nature* **426**, 517–524
40. Montell, C. (2005) The TRP superfamily of cation channels. *Sci. STKE* **2005**, re3
41. Dhaka, A., Viswanath, V., and Patapoutian, A. (2006) Trp ion channels and temperature sensation. *Annu. Rev. Neurosci.* **29**, 135–161
42. Hanson, S. M., Newstead, S., Swartz, K. J., and Sansom, M. S. P. (2015) Capsaicin interaction with TRPV1 channels in a lipid bilayer: Molecular dynamics simulation. *Biophys. J.* **108**, 1425–1434
43. Wen, H., Qin, F., and Zheng, W. (2016) Toward elucidating the heat activation mechanism of the TRPV1 channel gating by molecular dynamics simulation. *Proteins* **84**, 1938–1949
44. Wen, H., and Zheng, W. (2018) Decrypting the heat activation mechanism of TRPV1 channel by molecular dynamics simulation. *Biophys. J.* **114**, 40–52
45. Zheng, W., and Wen, H. (2019) Heat activation mechanism of TRPV1: New insights from molecular dynamics simulation. *Temperature (Austin)* **6**, 120–131
46. Morris, G. M., Goodsell, D. S., Halliday, R. S., Huey, R., Hart, W. E., Belew, R. K., and Olson, A. J. (1999) Automated docking using a Lamarckian genetic algorithm and an empirical binding free energy function. *J. Comput. Chem.* **19**, 1639–1662